Advances in Water Resources 117 (2018) 87–97

Contents lists available at ScienceDirect

Advances in Water Resources

journal homepage: www.elsevier.com/locate/advwatres

A new efficient implicit scheme for discretising the stiff friction terms in the shallow water equations

Xilin Xia[b,c], Qiuhua Liang[a,b,c,*]

[a] Hebei University of Engineering, Handan, China
[b] School of Engineering, Newcastle University, Newcastle upon Tyne, UK
[c] School of Architecture, Building and Civil Engineering, Loughborough University, Loughborough, UK

ARTICLE INFO

Keywords:
Shallow water equations
Friction source terms
Implicit scheme
Stiff relaxation
Overland flow
Finite volume method

ABSTRACT

Discretisation of the friction terms to ensure numerical stability and accuracy remains to be challenging for the development of robust numerical schemes to solve the shallow water equations (SWEs), particularly for applications involving very shallow flows (e.g. overland flows and wet/dry fronts) over complex domain topography. The key challenge is to ensure relaxation of the flow towards an equilibrium state characterised by the balance between friction and gravity in a computationally efficient way. To overcome this numerical challenge, this paper proposes a novel approach for discretising the friction source terms in the SWEs in the context of an explicit finite volume method. The overall numerical scheme adopts the HLLC Riemann solver and surface reconstruction method (SRM) to explicitly discretise the flux and bed slope source terms. Whilst a fully implicit scheme is used to handle the friction source terms, solution to the implicit formulation is analytically derived to explicitly update the flow variables. Compared with the existing approaches, the proposed scheme effectively resolves the issue associated with stiff relaxation without necessity to use an iteration method and it supports efficient simulation using time steps controlled only by the Courant–Friedrichs–Levy (CFL) condition. The current friction term discretisation scheme is not coupled with flux and bed slope calculation and therefore may be readily implemented in any other explicit finite volume SWE models. After being successfully validated against two benchmark tests with analytical solutions, the resulting new SWE model is applied to reproduce a rainfall-flooding event in the Upper Lee catchment in the UK.

1. Introduction

Many real-world examples of surface water flows, such as river flows, overland flows, flood waves and tsunamis, can be simulated by numerical models solving the shallow water equations (SWEs) (Berger et al., 2011; Di Giammarco et al., 1996; Kao and Chang, 2012; Sanders et al., 2010). In the past three decades, substantial progress has been made in developing numerical models to solve the SWEs and numerous robust numerical schemes have been developed and reported to address different issues related to real-world applications, for example, capturing the shock-like flow discontinuities (e.g. Toro, 2001), ensuring positivity of water depth for wetting and drying (e.g. Audusse et al., 2004; Liang and Marche, 2009) and preserving still water solutions (i.e. *C*-property) (e.g. Bermudez and Vazquez, 1994; Audusse et al., 2004; Hou et al., 2013; Murillo and García-Navarro, 2012a; Xing et al., 2011; Zhou et al., 2001).

However, proper discretisation of the friction source terms remains to be a challenge for developing numerically accurate and stable schemes to solve the SWEs for simulating very shallow flows as found in the applications involving overland flows and wet/dry fronts. As pointed out in Xia et al. (2017), inappropriate discretisation of the friction source terms may result in 1) numerical instability that leads to the use of prohibitive small time steps, and 2) inaccurate prediction of flow velocities.

In the SWE formulation, the friction terms are normally expressed as a non-linear function of velocity and flow depth. The Manning and Chezy formulae provide examples of the most commonly used friction laws (Chow, 1959). For example, the 1D SWEs may be formulated as

$$\frac{\partial h}{\partial t} + \frac{\partial hu}{\partial x} = 0, \tag{1}$$

$$\frac{\partial hu}{\partial t} + \frac{\partial (hu^2 + \frac{1}{2}gh^2)}{\partial x} = -ghS_b - S_f, \tag{2}$$

where h is the flow depth, u is the flow velocity in the x-direction, g is the acceleration due to gravity, S_b is the bed slope, and $S_f = gn^2h^{-\frac{1}{3}}u|u|$ is the friction source term expressed in the form of the Manning formula in which n is the Manning coefficient. It is the non-linear nature of the friction source terms and their interactions with other source terms

* Corresponding author.
E-mail addresses: xilin.xia@ncl.ac.uk (X. Xia), qiuhua.liang@ncl.ac.uk (Q. Liang).

https://doi.org/10.1016/j.advwatres.2018.05.004
Received 7 March 2018; Received in revised form 2 May 2018; Accepted 7 May 2018
Available online 8 May 2018

that bring in the major difficulty for developing robust discretisation schemes. We may consider a simple example of uniform flow on a slope to illustrate the physical behaviour of the friction terms. The direction of the friction is always opposite to the velocity/flow direction. If the friction is larger than the gravity component along the bed slope, the flow will be decelerated to have a reduced velocity; subsequently the friction, a function of flow velocity and depth, will also be reduced until a new balance is reached between the friction and gravity component. On the other hand, if the friction is smaller than the gravity component, the flow velocity, and hence the friction, will increase until a new balance is reached. Therefore, the friction source terms always take effect to relax the flow towards an equilibrium steady state characterised by the balance between the friction and gravity along the flow direction.

The timescale of the friction relaxation towards the equilibrium steady state may be estimated from the Jacobian matrix of the friction terms. For the 1D SWEs in Eqs. (1) and (2), it is given as (Xia et al., 2017)

$$T_f \sim \frac{1}{h^{-1}\left|\frac{\partial S_f}{\partial u}\right|} = \frac{1}{2gn^2h^{-\frac{4}{3}}|u|}. \tag{3}$$

Eq. (3) reveals that the relaxation time becomes small when the water depth is small, which may become much smaller than the time step determined by the Courant–Friedrichs–Levy (CFL) condition in an explicit SWE model. Such a quick relaxation is often referred to as "stiff" relaxation and linked to the so-called "stiff" friction source terms. To resolve the numerical issue related to stiff relaxation, a simple way would be to restrict the time step length. However, this may lead to the use of prohibitive small time steps and subsequently unrealistic long simulation time. Therefore, the specific challenge is to develop an effective numerical scheme for the friction source terms that can relax the flow towards the correct steady state using time steps solely determined by the CFL condition without further constraints.

In the past three decades, numerous attempts have been made to develop friction term discretisation schemes to achieve better numerical stability. But much less attention has been given to improving numerical accuracy and predicting the correct equilibrium state of the flows. To provide stable simulations, implicit schemes have been widely used to discretise the friction source terms (e.g. Fiedler and Ramirez, 2000; Liang et al., 2007; Cea et al., 2010; Song et al., 2011; Costabile et al., 2013; Simons et al., 2014; Busaman et al., 2015; Cea and Blade, 2015; Rousseau et al., 2015; Singh et al., 2015). Unlike the explicit schemes, implicit schemes use the velocities at the new time step to evaluate the friction terms. In other words, the velocities are assumed to have the values after relaxation. In this way, the implicit schemes intrinsically enforce the relaxation of the friction terms to take effect in the current time step, effectively removing the "stiffness" of the friction terms.

In order to simplify the numerical implementation of an implicit friction discretisation scheme, a popular way is to reformulate the friction terms into explicit formulations. For example, the schemes reported in Fiedler and Ramirez (2000) and Simons et al. (2014) expand the friction terms using the Taylor's series and omit the higher order terms to obtain an explicit formulation. Other researchers (e.g. Liang et al., 2007; Cea et al., 2010; Song et al., 2011; Costabile et al., 2013; Busaman et al., 2015; Cea and Blade, 2015; Rousseau et al., 2015; Singh et al., 2015) express the friction terms as the product of the velocity in the current time step and that in the new time step to obtain an explicit formula. Although these schemes may effectively avoid the numerical instability caused by the stiff friction terms, they commonly relax the flows to a wrong steady state, which may consequently lead to incorrect simulation results (Xia et al., 2017).

Based on the fact that the maximum effect of friction is to fully stop the flow, certain friction discretisation schemes (Burguete et al., 2008; Liang and Marche, 2009) also impose an upper bound on the friction so that it can only reduce the velocity to zero but not change its sign to reverse the flow. These schemes effectively force the friction to relax the flow velocity to zero, which is not necessarily the physically correct steady state. The value of the physically correct steady state velocity depends on the bed slope and is generally not zero. Furthermore, the flow direction may be reversed during a single time step under certain conditions. Taking the example of a flow moving uphill, the combined effect of friction and gravity will firstly decelerate the flow until it stops, and then the gravity will accelerate the flow downhill until it is balanced by the friction. The flow direction has actually been reversed and this process may theoretically happen in a single time step.

Through a different approach, the scheme proposed by Murillo and García-Navarro (2012b) integrates the discretisation of friction terms into the adopted Riemann solver. This approach essentially linearizes the friction terms when integrating them over the time. Since the approach does not explicitly consider the non-linear relaxation imposed by the friction terms, an additional fix must be implemented to ensure numerical stability and convergence to the steady state. Another disadvantage of this approach is that the discretisation of the friction source terms and flux terms are fully coupled and cannot be easily applied in other finite volume models that adopt different flux discretisation schemes.

Attempts have also been reported recently to develop numerical methods for proper relaxation of the stiff friction terms in SWE models. In Yu and Duan (2014), the flow velocity is adaptively set to a theoretical steady state value determined by the balance between the bed and friction slopes when the so-called kinematic wave number is larger than a threshold. This method was further improved by also considering the pressure gradient terms when determining the steady state velocity (Yu and Duan, 2017). However, the threshold for imposing steady state velocity, i.e. the kinematic wave number, is a case-dependent parameter, which restricts the robustness of the method for wider applications. More recently, Xia et al. (2017) introduced a fully implicit friction discretisation scheme that can effectively relax the flow towards the correct steady state and allow the use of CFL time step even when it is much bigger than the relaxation time scale. Different from the aforementioned schemes that reformulate the equations into an explicit form, Xia et al. (2017) directly solved the implicit friction equations using a Newton–Raphson iteration method. This, however, inevitably complicates the numerical implementation and potentially increases the computational cost.

Due to the various limitations of the existing approaches, this paper proposes a novel implicit scheme for discretising the friction source terms of the SWEs in the context of a finite volume method. The new scheme is able to relax the flow velocity towards the correct equilibrium steady state using a normal time step determined by the CFL condition even when it is much bigger than the relaxation time scale. Meanwhile, the new scheme calculates the friction terms explicitly without using an iteration method. It is therefore straightforward to implement and computationally more efficient. The rest of the paper is organised as follows: Section 2 presents the governing equations; Section 3 presents the numerical scheme with an emphasis on friction source term discretisation; Section 4 validates the resulting SWE model using carefully selected test cases before it is applied to reproduce a real-world rainfall event in Section 5; and finally, brief conclusions are drawn in Section 6.

2. Governing equations

The vectorised form of the 2D shallow water equations (SWEs) may be written as

$$\frac{\partial \boldsymbol{q}}{\partial t} + \frac{\partial \boldsymbol{f}}{\partial x} + \frac{\partial \boldsymbol{g}}{\partial y} = \boldsymbol{S}_b + \boldsymbol{S}_f \tag{4}$$

where $\boldsymbol{q}$ contains the conserved flow variables, $\boldsymbol{f}$ and $\boldsymbol{g}$ are the x- and y-direction flux vector terms, and $\boldsymbol{S}_b$ and $\boldsymbol{S}_f$ are the source terms representing respectively the bed slope and friction effects. These vector

terms are given by

$$\boldsymbol{q}=\begin{bmatrix} h \\ hu \\ hv \end{bmatrix},\ \boldsymbol{f}=\begin{bmatrix} uh \\ u^2h+\frac{1}{2}gh^2 \\ uvh \end{bmatrix},\ \boldsymbol{g}=\begin{bmatrix} vh \\ uvh \\ v^2h+\frac{1}{2}gh^2 \end{bmatrix}, \tag{5}$$

$$\boldsymbol{S}_b=\begin{bmatrix} 0 \\ -gh\frac{\partial b}{\partial x} \\ -gh\frac{\partial b}{\partial y} \end{bmatrix}, \boldsymbol{S}_f=\begin{bmatrix} 0 \\ -\frac{\tau_{bx}}{\rho} \\ -\frac{\tau_{by}}{\rho} \end{bmatrix}, \tag{6}$$

where v is the depth-averaged velocity component in the y-directions, ρ is the water density, and τ_{bx} and τ_{by} are the friction stresses calculated using the Manning equation:

$$\tau_{bx}=\rho C_f u\sqrt{u^2+v^2},\quad \tau_{by}=\rho C_f v\sqrt{u^2+v^2}, \tag{7}$$

with

$$C_f=\frac{gn^2}{h^{\frac{1}{3}}}. \tag{8}$$

It is worth noting that the SWEs are generally not applicable to flows on steep slopes and modifications to the original formulation have been proposed to resolve this issue (e.g. Juez et al., 2013, 2014; Xia and Liang, 2018). The friction term discretisation scheme proposed in this work can be trivially adapted for use in these modified SWEs.

3. Numerical scheme

The above 2D SWEs are solved using a first-order Godunov-type finite volume method. The adopted numerical scheme is presented in this section with an emphasis on the introduction of the proposed new discretisation scheme for the friction source terms.

3.1. First-order Godunov-type finite volume method

The time-marching scheme for the finite volume method is given as follows

$$\boldsymbol{q}^{n+1}=\boldsymbol{q}^n-\frac{\Delta t}{\Omega_i}\sum_{k=1}^{N}\boldsymbol{F}_k(\boldsymbol{q}^n)l_k+\Delta t\left(\boldsymbol{R}_i^n+\boldsymbol{S}_{bi}^n+\boldsymbol{S}_{fi}^{n+1}\right), \tag{9}$$

in which subscripts i and k are the indices of a cell and the cell edges, superscript n denotes the time level, $\boldsymbol{F}_k(\boldsymbol{q})$ contains the fluxes normal to cell edge k, l_k is the length of the cell edge k, Ω_i is the cell area, and Δt is the time step. In the current numerical scheme, the flux and slope source terms are discretised explicitly based on the flow variables at time level n. But the friction source terms are discretised implicitly using the flow variables at time level $n+1$.

3.2. Calculation of flux and bed slope source terms

In this work, the flux term $\boldsymbol{F}_k(\boldsymbol{q})$ is calculated using an HLLC Riemann solver, for which the details can be found in Toro (2001). The required Riemann states are obtained using the surface reconstruction method (SRM) as proposed by Xia et al. (2017). SRM firstly reconstructs the water surface elevations at the left and right-hand sides of a given cell interface. Considering two adjacent cells i and $i+1$, the reconstructed water surface elevations (denoted by η) are

$$\eta_L=\eta_i+\max\left[0,\min\left(b_{i+1}-b_i-\delta b,\eta_{i+1}-\eta_i\right)\right], \tag{10}$$

$$\eta_R=\eta_{i+1}+\max\left[0,\min\left(b_i-b_{i+1}+\delta b,\eta_i-\eta_{i+1}\right)\right], \tag{11}$$

with

$$\delta b=b_{i+1/2+}-b_{i+1/2-}, \tag{12}$$

in which $b_{i+1/2-}$ and $b_{i+1/2+}$ are the bed elevations at the left and right-hand sides of the cell interface, which are interpolated from the corresponding cell-centre values using a slope limited method as

$$b_{i+1/2-}=b_i+\boldsymbol{r}_i\nabla b_i \text{ and } b_{i+1/2+}=b_{i+1}+\boldsymbol{r}_{i+1}\nabla b_{i+1}, \tag{13}$$

where $\boldsymbol{r}$ is the distance vector from the cell centre to the cell interface and ∇b is the slope limited gradient of bed elevation. In this work, the widely used minmod slope limiter is adopted for numerically stable simulations.

The bed elevations at the left and right-hand sides of the cell interface are then redefined using the corresponding reconstructed water surface elevations and water depths as

$$\begin{cases} b_L=\eta_L-h_i \\ b_R=\eta_R-h_{i+1} \end{cases}, \tag{14}$$

which are then used to define a single bed elevation at the cell interface as

$$b_f=\max\left(b_L,b_R\right), \tag{15}$$

based on which the Riemann states of the flow depth are defined

$$\begin{cases} h_L=\max\left(0,\eta_L-b_f\right) \\ h_R=\max\left(0,\eta_R-b_f\right) \end{cases}. \tag{16}$$

The Riemann states of the discharges are subsequently deduced

$$\begin{cases} [hu]_L=h_Lu_i \\ [hu]_R=h_Ru_{i+1} \end{cases}, \begin{cases} [hv]_L=h_Lv_i \\ [hv]_R=h_Rv_{i+1} \end{cases}, \tag{17}$$

where $u_i=[hu]_i/h_i$ and $v_i=[hv]_i/h_i$ (similarly u_{i+1} and v_{i+1}) are the depth-averaged velocities calculated at the cell centres.

These Riemann states are then used to calculate the numerical fluxes in Eq. (9) using an HLLC Riemann solver in the context of the first-order Godunov-type finite volume method as adopted in this work. The bed slope source terms are calculated as

$$S_{bi}=\begin{pmatrix} 0 \\ \frac{1}{\Omega_i}\sum\frac{1}{2}g\left(h_i+h_{L,k}\right)\left(b_i-\bar{b}_{f,k}\right)\boldsymbol{n}_kl_k \end{pmatrix} \tag{18}$$

where $h_{L,k}$ is the left Riemann state of the flow depth at cell edge 'k', and $\bar{b}_{f,k}$ is defined as

$$\bar{b}_f=b_f-\Delta b, \tag{19}$$

$$\begin{cases} \Delta b=\max\left(0,b_f-\eta_i\right) & \text{if } h_{i+1}<\varepsilon_h \\ \Delta b=\max\left[0,\min\left(\delta b,b_f-\eta_i\right)\right] & \text{if } h_{i+1}\geq\varepsilon_h \end{cases}, \tag{20}$$

in which $\epsilon_h=10^{-10}$ is a small value to define a dry cell. The present flux and slope discretisation schemes automatically ensure non-negative water depth and preserve still water solutions (i.e. C-property) for simulations involving wetting and drying over rough terrain with complex topography (Xia et al., 2017).

3.3. Discretisation of the friction source terms

In the current Godunov-type finite volume scheme, the friction source terms in Eq. (9) are discretised implicitly, but the actual calculation is carried out explicitly through derivation of an effective explicit formulation. To derive the required explicit formulation, the momentum components in Eq. (9) are firstly expanded into a scalar form as

$$q_x^{n+1}=q_x^n+\Delta tA_x-\Delta tgn^2(h^n)^{-\frac{7}{3}}q_x^{n+1}\sqrt{\left(q_x^{n+1}\right)^2+\left(q_y^{n+1}\right)^2}, \tag{21}$$

$$q_y^{n+1}=q_y^n+\Delta tA_y-\Delta tgn^2(h^n)^{-\frac{7}{3}}q_y^{n+1}\sqrt{\left(q_x^{n+1}\right)^2+\left(q_y^{n+1}\right)^2}, \tag{22}$$

in which $q_x=hu$ and $q_y=hv$ are the x- and y-direction components of the unit-width discharge, and A_x and A_y represent the momentum components of $-\frac{1}{\Omega_i}\sum_{k=1}^{N}\boldsymbol{F}_k(\boldsymbol{q}^n)l_k+\boldsymbol{S}_{bi}^n$ respectively in the x- and y-directions.

Eqs. (21) and (22) are obviously non-linear functions of q_x^{n+1} and q_y^{n+1}. To find the roots for q_x^{n+1} and q_y^{n+1}, a new approach is proposed and implemented in this work to analytically solve Eqs (21) and (22), instead of using the Newton–Raphson iteration method as reported in Xia et al. (2017). Firstly, Eqs (21) and (22) are reformulated into

$$q_x^{n+1}\left[1+\Delta t g n^2 (h^n)^{-\frac{7}{3}}\sqrt{\left(q_x^{n+1}\right)^2+\left(q_y^{n+1}\right)^2}\right]=q_x^n+\Delta t A_x \tag{23}$$

$$q_y^{n+1}\left[1+\Delta t g n^2 (h^n)^{-\frac{7}{3}}\sqrt{\left(q_x^{n+1}\right)^2+\left(q_y^{n+1}\right)^2}\right]=q_y^n+\Delta t A_y \tag{24}$$

Dividing Eq. (23) by Eq. (24) leads to

$$\frac{q_x^{n+1}}{q_y^{n+1}}=\frac{q_x^n+\Delta t A_x}{q_y^n+\Delta t A_y}. \tag{25}$$

Then by substituting (25) into (23), we can obtain

$$q_x^{n+1}\left[1+\Delta t g n^2 (h^n)^{-\frac{7}{3}}\sqrt{\left(q_x^{n+1}\right)^2+\left(\frac{m_y}{m_x}\right)^2\left(q_x^{n+1}\right)^2}\right]=m_x, \tag{26}$$

in which

$$m_x=q_x^n+\Delta t A_x \text{ and } m_y=q_y^n+\Delta t A_y. \tag{27}$$

If q_x^{n+1} is positive, Eq. (26) may be rewritten as

$$q_x^{n+1}+(q_x^{n+1})^2\Delta t g n^2 (h^n)^{-\frac{7}{3}}\sqrt{1+\left(\frac{m_y}{m_x}\right)^2}=m_x. \tag{28}$$

Otherwise,

$$q_x^{n+1}-(q_x^{n+1})^2\Delta t g n^2 (h^n)^{-\frac{7}{3}}\sqrt{1+\left(\frac{m_y}{m_x}\right)^2}=m_x. \tag{29}$$

Eqs (28) and (29) are quadratic equations in terms of q_x^{n+1}, and each of them has two roots. Therefore, mathematically there may be as many as four roots for Eq. (26) (two for the positive q_x^{n+1} and two for the non-positive q_x^{n+1}). However, only one of these roots is physically meaningful for hydrodynamic modelling, which must be correctly identified. The two roots for Eq. (28), i.e. the positive q_x^{n+1}, are

$$q_x^{n+1}=\frac{1+\sqrt{1+4\Delta t g n^2 (h^n)^{-\frac{7}{3}} m_x\sqrt{1+\left(\frac{m_y}{m_x}\right)^2}}}{-2\Delta t g n^2 (h^n)^{-\frac{7}{3}}\sqrt{1+\left(\frac{m_y}{m_x}\right)^2}} \tag{30}$$

and

$$q_x^{n+1}=\frac{1-\sqrt{1+4\Delta t g n^2 (h^n)^{-\frac{7}{3}} m_x\sqrt{1+\left(\frac{m_y}{m_x}\right)^2}}}{-2\Delta t g n^2 (h^n)^{-\frac{7}{3}}\sqrt{1+\left(\frac{m_y}{m_x}\right)^2}} \tag{31}$$

And the two roots for Eq. (29), i.e. the non-positive q_x^{n+1}, are

$$q_x^{n+1}=\frac{1+\sqrt{1-4\Delta t g n^2 (h^n)^{-\frac{7}{3}} m_x\sqrt{1+\left(\frac{m_y}{m_x}\right)^2}}}{2\Delta t g n^2 (h^n)^{-\frac{7}{3}}\sqrt{1+\left(\frac{m_y}{m_x}\right)^2}} \tag{32}$$

and

$$q_x^{n+1}=\frac{1-\sqrt{1-4\Delta t g n^2 (h^n)^{-\frac{7}{3}} m_x\sqrt{1+\left(\frac{m_y}{m_x}\right)^2}}}{2\Delta t g n^2 (h^n)^{-\frac{7}{3}}\sqrt{1+\left(\frac{m_y}{m_x}\right)^2}} \tag{33}$$

Which one of the above four roots is physically admissible for hydrodynamic modelling depends on m_x. If m_x is positive, Eq. (30) is negative, which contradicts to the prescribed assumption of positive q_x^{n+1} (i.e. $q_x^{n+1}>0$); on the other hand, Eq. (31) is positive, which is consistent with assumption of $q_x^{n+1}>0$. Meanwhile, Eqs (32) and (33) are both positive as long as they are real, which are clearly not consistent with the assumption of $q_x^{n+1}\le 0$. Therefore, Eq. (31) provides the only physically correct root for Eq. (29) if $m_x>0$. Similarly, we can prove that Eq. (33) gives the only admissible root for Eq. (29) if $m_x<0$. These two admissible roots can be combined into one analytical expression as

$$q_x^{n+1}=\frac{m_x-m_x\sqrt{1+4\Delta t g n^2 (h^n)^{-\frac{7}{3}}\sqrt{m_x^2+m_y^2}}}{-2\Delta t g n^2 (h^n)^{-\frac{7}{3}}\sqrt{m_x^2+m_y^2}}. \tag{34}$$

If h^n is excessively small (e.g. near to the wet-dry front), the term $(h^n)^{-\frac{7}{3}}$ may return an exaggerating big value ($\sim 10^{20}$ depending on the value water depth) that may exceed the maximum machine precision and thus create machine error leading to numerical stability. To avoid this, part of $(h^n)^{-\frac{7}{3}}$ is cast into the square root operators to facilitate stable numerical implementation and the final expression for q_x^{n+1} is given as

$$q_x^{n+1}=\frac{m_x-m_x\sqrt{1+4\Delta t g n^2 (h^n)^{-\frac{4}{3}}\sqrt{\left(\frac{m_x}{h^n}\right)^2+\left(\frac{m_y}{h^n}\right)^2}}}{-2\Delta t g n^2 (h^n)^{-\frac{4}{3}}\sqrt{\left(\frac{m_x}{h^n}\right)^2+\left(\frac{m_y}{h^n}\right)^2}} \tag{35}$$

It is also possible that the denominator may return a zero, making Eq. (35) to become singular. In such a case, $q_x^{n+1}=m_x$ is effectively the root to (29). To avoid singularity in the numerical calculation, Eq. (34) is slightly modified to become

$$q_x^{n+1}=\begin{cases} m_x, & \text{if } \Delta t g n^2 (h^n)^{-\frac{4}{3}}\sqrt{\left(\frac{m_x}{h^n}\right)^2+\left(\frac{m_y}{h^n}\right)^2}<10^{-10} \\ \dfrac{m_x-m_x\sqrt{1+4\Delta t g n^2 (h^n)^{-\frac{4}{3}}\sqrt{\left(\frac{m_x}{h^n}\right)^2+\left(\frac{m_y}{h^n}\right)^2}}}{-2\Delta t g n^2 (h^n)^{-\frac{4}{3}}\sqrt{\left(\frac{m_x}{h^n}\right)^2+\left(\frac{m_y}{h^n}\right)^2}}, & \text{if } \Delta t g n^2 (h^n)^{-\frac{4}{3}}\sqrt{\left(\frac{m_x}{h^n}\right)^2+\left(\frac{m_y}{h^n}\right)^2}\ge 10^{-10} \end{cases} \tag{36}$$

Similarly, the physically admissible root for Eq. (24) and the final expression for q_y^{n+1} can be derived and given as follows

$$q_y^{n+1}=\begin{cases} m_y, & \text{if } \Delta t g n^2 (h^n)^{-\frac{4}{3}}\sqrt{\left(\frac{m_x}{h^n}\right)^2+\left(\frac{m_y}{h^n}\right)^2}<10^{-10} \\ \dfrac{m_y-m_y\sqrt{1+4\Delta t g n^2 (h^n)^{-\frac{4}{3}}\sqrt{\left(\frac{m_x}{h^n}\right)^2+\left(\frac{m_y}{h^n}\right)^2}}}{-2\Delta t g n^2 (h^n)^{-\frac{4}{3}}\sqrt{\left(\frac{m_x}{h^n}\right)^2+\left(\frac{m_y}{h^n}\right)^2}}, & \text{if } \Delta t g n^2 (h^n)^{-\frac{4}{3}}\sqrt{\left(\frac{m_x}{h^n}\right)^2+\left(\frac{m_y}{h^n}\right)^2}\ge 10^{-10} \end{cases}. \tag{37}$$

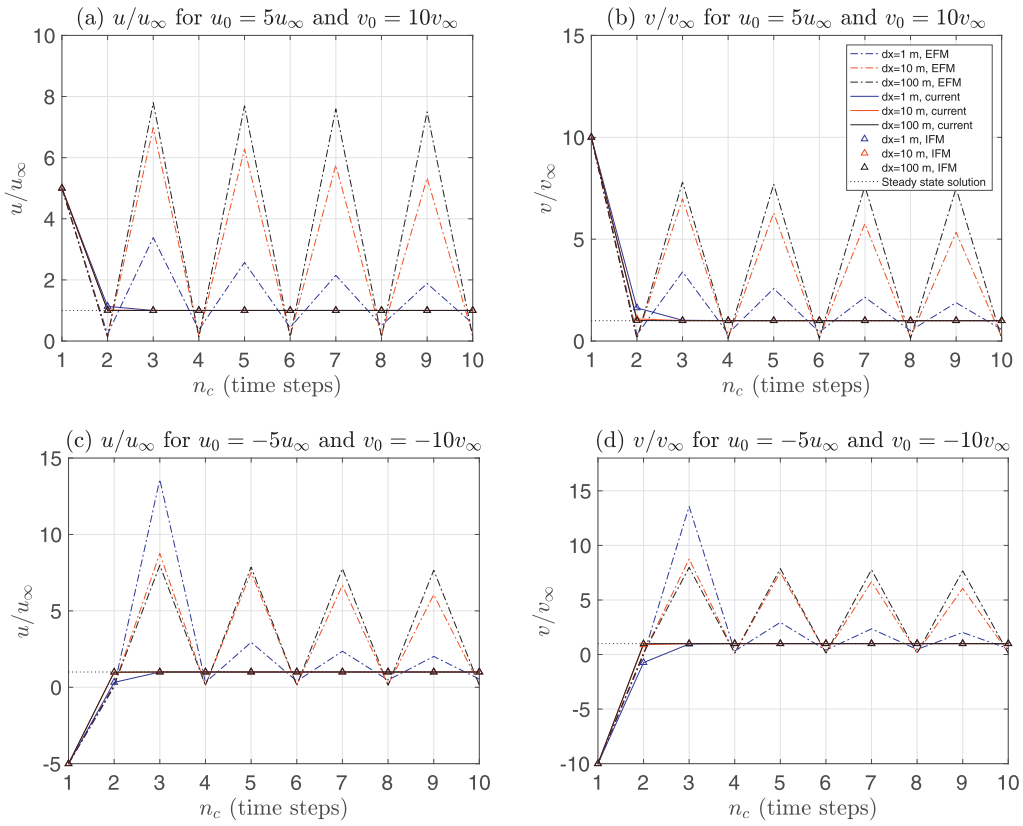

Fig. 1. Comparison of flow velocities predicted by different numerical schemes on different grids: (a) x-direction velocity for case A; (b) y-direction velocity for case A; (c) x-direction velocity for case B; (d) y-direction velocity for case B. The plotted velocities are normalised against the steady state velocities.

Therefore, the explicit expressions of q_x^{n+1} and q_y^{n+1} accounting for the friction effects are given by Eq. (36) and Eq. (37), which can be explicitly calculated and incorporated into the adopted Godunov-type scheme to develop a new SWE model.

In order to mathematically prove that the proposed numerical scheme can effectively relax the flow velocity to the correct equilibrium steady state, we consider $\Delta t \to \infty$ in Eq. (36) and Eq. (37). By assuming $\Delta t \to \infty$, we effectively impose that the CFL-determined time step is much bigger than the relaxation time scale. The resulting expressions for q_x^{n+1} and q_y^{n+1} become

$$\lim_{\Delta t \to \infty} q_x^{n+1} = \frac{A_x}{\sqrt{gn^2 (h^n)^{-\frac{7}{3}} \sqrt{A_x^2 + A_y^2}}}, \tag{38}$$

$$\lim_{\Delta t \to \infty} q_y^{n+1} = \frac{A_y}{\sqrt{gn^2 (h^n)^{-\frac{7}{3}} \sqrt{A_x^2 + A_y^2}}}. \tag{39}$$

Apparently, $\lim_{\Delta t \to \infty} q_x^{n+1}$ and $\lim_{\Delta t \to \infty} q_y^{n+1}$ are the unit-width discharges determined by the balance between the friction and other terms (i.e. the flux and bed slope terms) in the SWEs. Therefore, the physically correct equilibrium steady state can be properly recovered by the proposed friction discretisation scheme. It should be also noted that $\lim_{\Delta t \to \infty} q_x^{n+1}$ and $\lim_{\Delta t \to \infty} q_y^{n+1}$ do not necessarily have the same signs as q_x^n and q_y^n. This defies the assumption adopted by Burguete et al. (2008) and Liang and Marche (2009), where the flow direction cannot be reversed within a single time step. In the current friction discretisation scheme, the flow can theoretically be reversed during a time step.

3.4. Solution procedure

At each time step, the solution procedure of the resulting SWE model may be summarised as follows:

(1) Explicitly evaluate the flux terms and bed slope source terms using SRM as described in section 3.2;
(2) Integrate the mass flux term in Eq. (9) to obtain h^{n+1};
(3) Integrate the momentum flux terms and the bed slope source terms in Eq. (27) to obtain m_x and m_y;
(4) Integrate the friction source terms in Eqs. (36) and (37) to respectively obtain q_x^{n+1} and q_y^{n+1};
(5) Update the flow variables and move to the next time step.

3.5. Stability criterion

For the resulting SWE model as introduced in the previous subsections, the time step length for numerically stable simulations is solely determined by the Courant–Friedrichs–Levy (CFL) condition given as

$$\Delta t = \mathrm{CFL} \frac{d_i}{|\boldsymbol{u}_i| + \sqrt{gh}} \tag{40}$$

where d_i is the minimum distance from the cell centre to the corresponding cell edges and CFL denotes the CFL number that takes a non-zero value between 0 and 1. CFL = 1.0 is used in all of the simulations in this work.

The stability criterion for the overall explicit SWE model is irrelevant to the friction term discretisation. This is because the flux and bed source terms and the friction source terms are treated separately. The new implicit friction term integration method proposed in this work relaxes the flow velocity to the correct equilibrium state even when the time step is large ($\Delta t \to \infty$), which effectively avoids further constraint

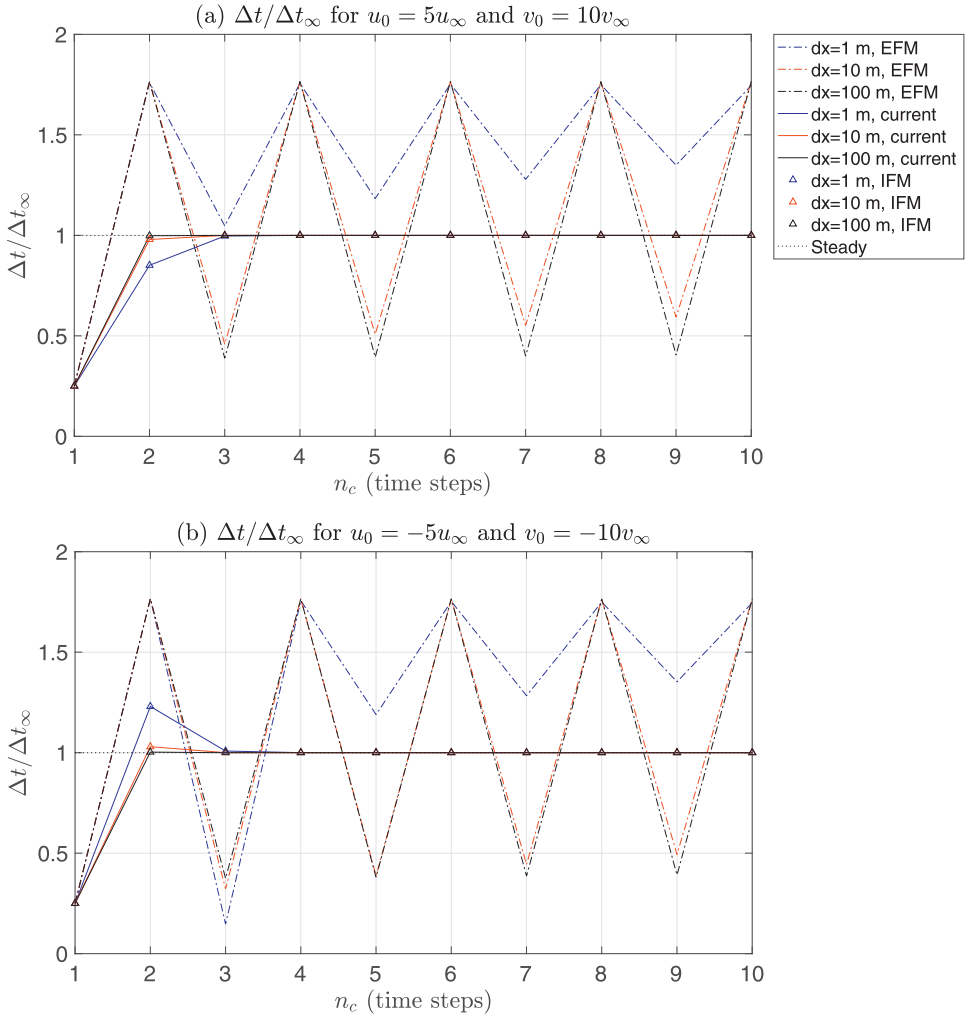

Fig. 2. Time steps used by different numerical schemes on different grids: (a) case A; (b) case B. The time steps are normalised against Δt_∞, calculated from u_∞ and v_∞ with CFL = 1.0.

on the time step length. Therefore, the time step of the overall model is only controlled by the CFL condition.

4. Model validation

Two analytical test cases are considered in this section to validate the new friction term discretisation scheme. Both test cases involve very small water depth to highlight the need of a proper numerical scheme to discretise the friction source terms for stable and accurate simulations. It is noteworthy that the discretisation scheme for flux and slope source terms have already been intensively tested and verified in our previous work (Xia et al., 2017). In particular, the scheme has been proven to perfectly preserve the lake at rest resolutions and ensure the positivity of water depths for applications involving complex topography and wetting and drying. Repeating these tests is deemed to be unnecessary and will not be considered herein.

To demonstrate the advantages of the new implicit friction discretisation scheme, the simulation results are compared with the analytical solutions and also numerical solutions obtained using two alternative schemes: 1) the iterative implicit scheme proposed by Xia et al. (2017), referred to as 'Iterative Friction Model (IFM)' herein; and 2) a popular implicit scheme adopted by many researchers (e.g. Busaman et al., 2015; Cea and Blade, 2015; Liang et al., 2006; Song et al., 2011), named as 'Explicit Friction Model (EFM)' from now on. The convergence criterion of IFM is chosen to be the same as that in Xia et al. (2017), i.e. the iteration stops when the relative difference between the solutions in two iterations is less than 0.001. EFM reformulates the implicit friction discretisation scheme into an explicit form as

$$q_x^{n+1} = \frac{m_x}{1 + \Delta t g n^2 (h^n)^{-\frac{4}{3}} \sqrt{(u^n)^2 + (v^n)^2}}, \tag{41}$$

and

$$q_y^{n+1} = \frac{m_y}{1 + \Delta t g n^2 (h^n)^{-\frac{4}{3}} \sqrt{(u^n)^2 + (v^n)^2}}. \tag{42}$$

To quantitatively assess the accuracy of the numerical simulation results, the root mean square error (RMSE) is defined and calculated by

$$RMSE = \sqrt{\frac{\sum_1^N \left(f_m^n - f_t^n\right)^2}{N}}, \tag{43}$$

where N is the total number of time steps, f_m^n is the simulated results, and f_t^n is the reference solutions for a specific flow variable f at $t = n$. Analytical solutions are available for comparison for both of the test cases considered in this section.

4.1. Two-dimensional uniform flow

The first test case to consdier is a 2D uniform flow with constant depth and velocity over a slope. The water depth is 0.001 m and the

Table 1
RMSEs of the predicted velocities against the steady state solutions.

	u/u_∞ for case A	v/v_∞ for case A	u/u_∞ for case B	v/v_∞ for case B
$\Delta x = 1$ m, EFM	1.16E + 00	1.15E + 00	4.32E + 00	4.31E + 00
$\Delta x = 10$ m, EFM	3.47E + 00	3.47E + 00	4.27E + 00	4.27E + 00
$\Delta x = 100$ m, EFM	4.48E + 00	4.48E + 00	4.60E + 00	4.60E + 00
$\Delta x = 1$ m, current	4.50E−02	2.09E−01	2.26E−01	5.79E−01
$\Delta x = 10$ m, current	3.98E−03	2.80E−02	8.97E−03	3.59E−02
$\Delta x = 100$ m, current	3.85E−04	2.92E−03	8.94E−04	3.46E−03
$\Delta x = 1$ m, IFM	4.50E−02	2.09E−01	2.26E−01	5.79E−01
$\Delta x = 10$ m, IFM	3.98E−03	2.80E−02	8.97E−03	3.59E−02
$\Delta x = 100$ m, IFM	3.85E−04	2.92E−03	8.94E−04	3.46E−03

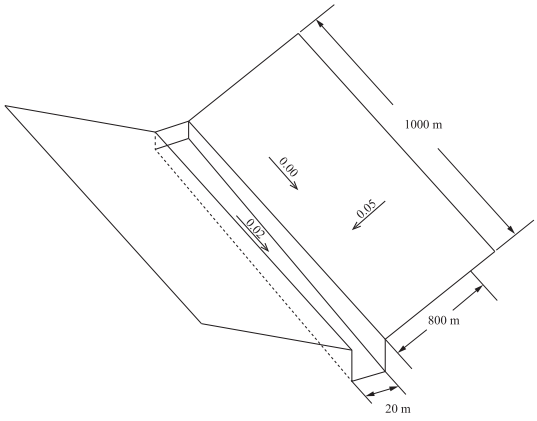

Fig. 3. Geometry of the V-shaped catchment.

bed slopes in the x- and y-directions, i.e. S_{bx} and S_{by}, are both 0.05. The Manning coefficient is taken as 0.035 $sm^{-1/3}$ and is constant over the entire domain. According to Xia et al. (2017), the steady state velocity components determined by the balance between friction and gravity are given by

$$u_\infty = \frac{S_{bx}}{\sqrt{gn^2h^{-\frac{1}{3}}\sqrt{\left(S_{bx}^2 + S_{by}^2\right)}}} \text{ and } v_\infty = \frac{S_{by}}{\sqrt{gn^2h^{-\frac{1}{3}}\sqrt{\left(S_{bx}^2 + S_{by}^2\right)}}}, \quad (44)$$

which give $u_\infty = 0.0537$ m/s and $v_\infty = 0.0537$ m/s based on the parameters as provided. Herein, two sets of initial velocities are considered, i.e. case A: $u_0 = 5u_\infty$, $v_0 = 10v_\infty$ and case B: $u_0 = -5u_\infty$, $v_0 = -10v_\infty$. The two sets of initial velocities have opposite signs to confirm the correct solutions to the two different quadratic equations resulting from Eq. (26). Three different grid sizes, i.e. $\Delta x = 1$ m, 10 m and 100 m, are used in the simulations.

The velocities predicted by the three different friction discretisation schemes are normalised by the theoretical steady state velocity and compared with each other in Fig. 1. The current scheme and IFM are both able to relax the flow velocity towards the correct steady state velocity monotonically in one or two time steps in all three simulations with different grid resolutions. It is worth noting that, for case B, the signs of both of the x- and y-direction steady state velocities are different from the initial conditions (i.e. the steady state velocities are positive while the initial velocities are negative, which can be clearly seen in Fig. 1(c) and (d)). The change of the signs of the velocities, subsequently the reversal of the flow, is predicted within a single time step by the current scheme and IFM for the coarse-grid simulations ($\Delta x = 10$ m and 100 m). This confirms the previous statement that the flow direction can be theoretically reversed within a single time step. The time steps used in the simulations are also plotted in Fig. 2 and comparable with Δt_∞ calculated from u_∞ and v_∞ with CFL = 1.0. This effectively demonstrates that stable and accurate simulations are achieved using time steps determined solely by the CFL condition. The current scheme provides numerical predictions identical to those by IFM, which is as expected and confirms the validity of the explicit friction formulae derived in the previous section. However, the flow velocities predicted by EFM fail to converge to the correct steady state on all three grid configurations.

Table 2
Discharge RMSEs calculated by different friction term discretisation schemes.

	Hillside discharge (m^3/s)	Channel outlet discharge (m^3/s)
EFM	0.0474	0.2391
IFM	0.0464	0.2377
current	0.0464	0.2377

The prediction accuracy of the three different schemes is quantified by calculating RMSEs, which are listed in Table 1. For all of the simulations, the RMSEs predicted by the current scheme and IFM are much smaller than those resulting from EFM. For the current scheme and IFM, the RMSEs decrease as the grid cell size increases, indicating that the flow is relaxed to the steady state with fewer time steps on coarser grids. This is consistent with the mathematical property of the Manning's friction terms. The relaxation scale is independent of the cell size as indicated by Eq. (3), but the time step length increases as the cell size increases. Therefore, fewer time steps are required to converge the flow to the steady state.

4.2. Overland flow on an idealised V-shaped catchment

The current friction discretisation scheme is further tested through simulating overland flow on an idealised V-shaped catchment. The catchment comprises of two hillsides with a 0.05 slope and a channel with a 0.02 slope, as shown in Fig. 3. The Manning coefficients for the hillslopes and channel are 0.015 $sm^{-1/3}$ and 0.15 $sm^{-1/3}$, respectively. Constant and uniform rainfall with an intensity of 10.8 mm/h falls on the whole catchment for 1.5 h from the beginning. Except for the channel outlet where open boundary conditions are imposed, all other boundaries are closed. A uniform grid of 10 m resolution is used for all of the simulations.

Fig. 4 presents the discharge hydrographs predicted by all of the three friction term discretisation schemes at the hillsides and channel outlet, which are compared with the analytical solutions derived based on the kinematic wave assumptions (see *Di* Giammarco et al., 1996 for details). The results produced by the current scheme and IFM are identical, which are all in good agreement with the analytical solutions. However, the hillside discharge predicted by the EFM scheme presents unphysical oscillations at the onset stage. This is directly caused by the small relaxation time for the very shallow overland flow on the hillside. In such a case, EFM cannot properly relax the flow velocity towards the correct steady state. The superiority of the current scheme and IFM is further confirmed by the calculated RMSEs listed in Table 2. The RMSEs resulting from the current scheme and IFM are slightly smaller than EFM for both the hillside and channel outlet discharges.

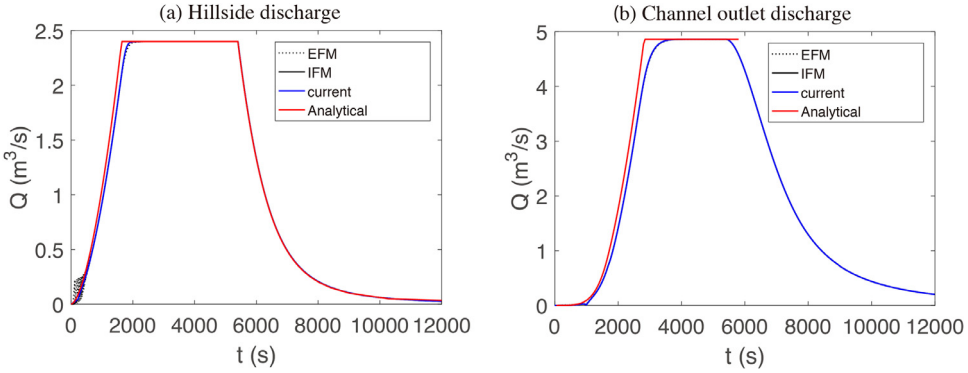

Fig. 4. Rainfall induced discharge hydrographs obtained: (a) on one of the hillside; (b) at the channel outlet.

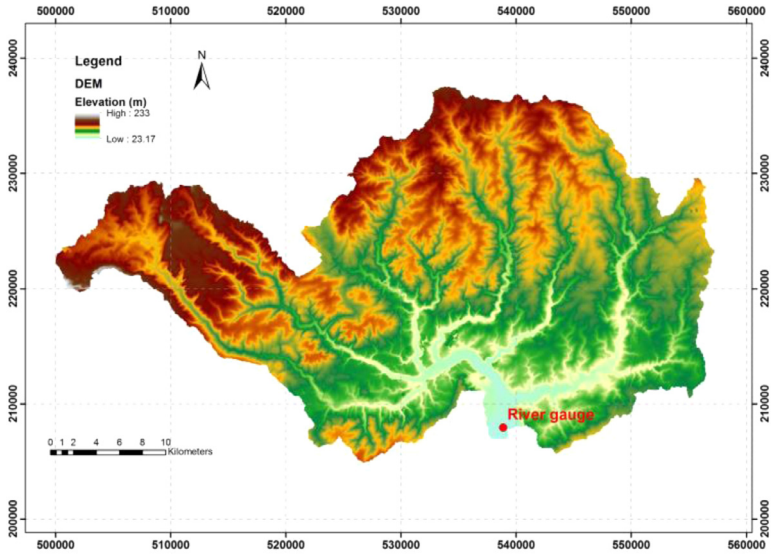

Fig. 5. Topographic map of the Upper Lee catchment.

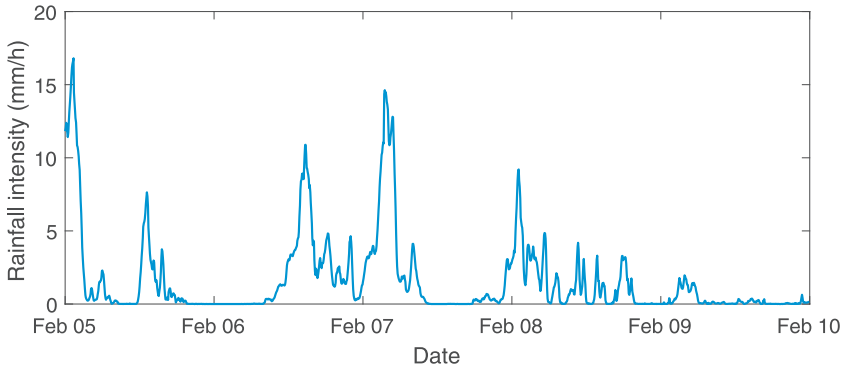

Fig. 6. Time series of the mean rainfall intensity over the catchment.

5. Application to a real-world rainfall-flooding event

In this section, the model implemented with the new friction discretisation scheme is applied to reproduce a rainfall-flooding event in the Upper Lee catchment at north London, UK. The catchment covers an area of 1180 km^2, as shown in Fig. 5. The records of catchment outlet discharge are available from a gauge station installed at the River Lee. Heavy rainfall was recorded between 5th and 11th Feb 2014, which directly triggered a flood event. The time series of the mean rainfall intensity over the whole catchment is presented in Fig. 6, showing several rainfall peaks. Although various uncertainties exist when assessing accuracy of a model for real-world applications, this test case is considered to validate the numerical stability and efficiency of the proposed numerical scheme for complex problems.

The simulation is carried out for a total of 120 h from 00:00 on 5th Feb 2014. The whole catchment is discretised using a uniform grid of 20 m resolution, leading to 2.95 million computational cells. Zero infiltration is assumed due to antecedent rainfall and saturated soil condition. The Manning coefficients are set to be spatially varying according to the land use types as shown in Fig. 7. The Manning coefficients for different land use types are summarised in Table 3, selected based on the commonly used values as suggested in Chow (1959). Since the pur-

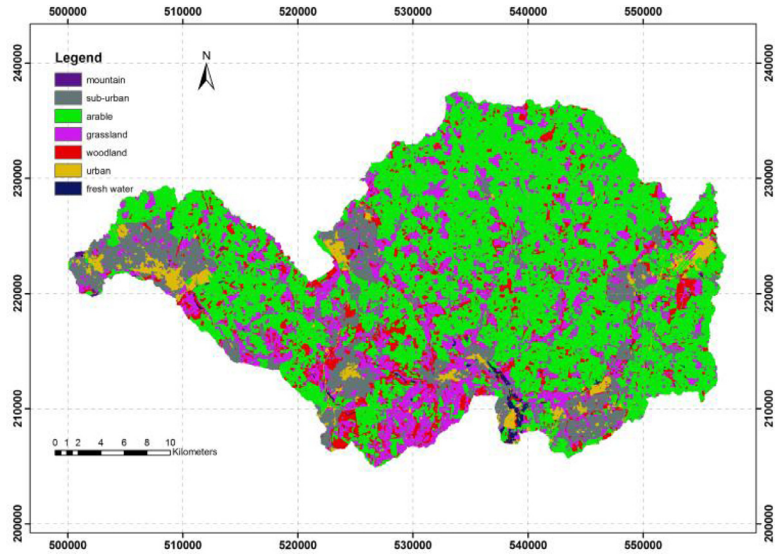

Fig. 7. Land use map of the Upper Lee catchment.

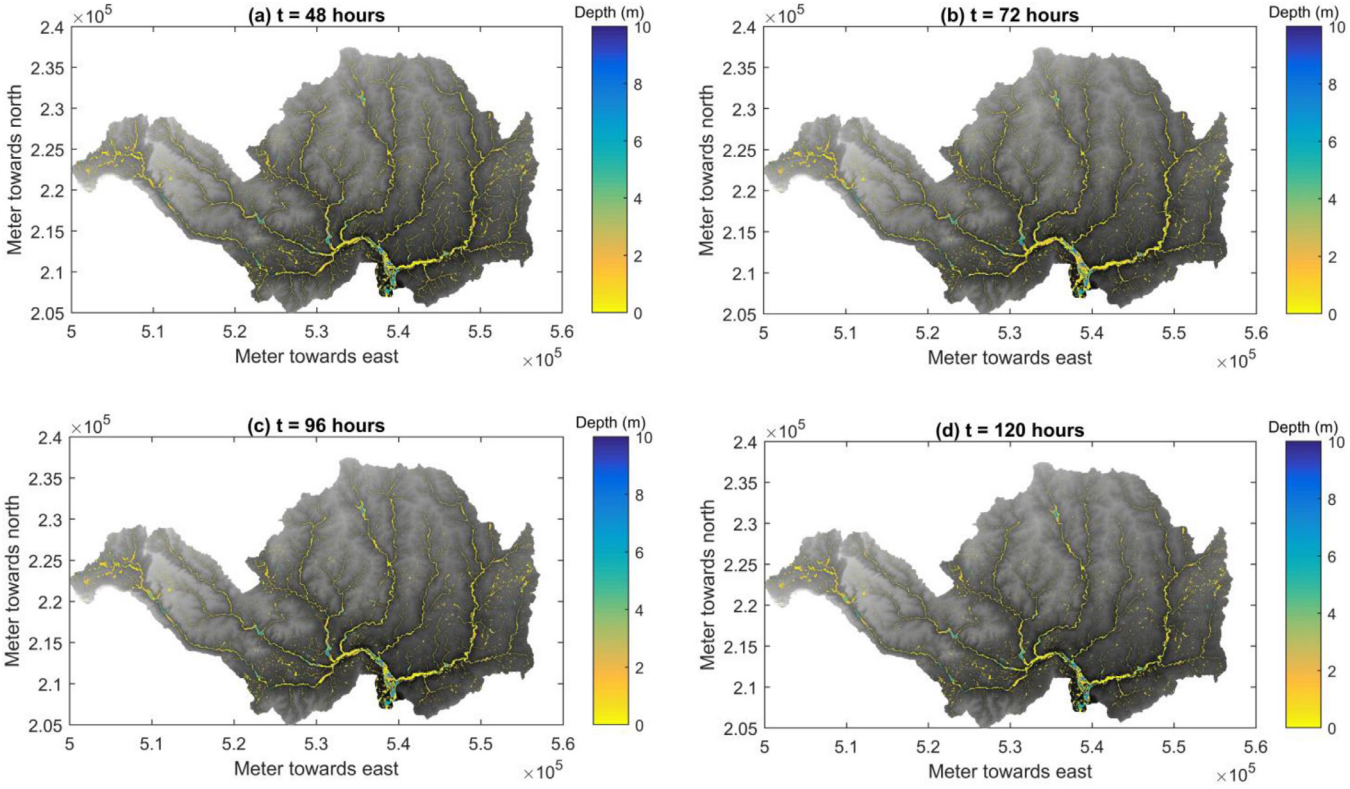

Fig. 8. Predicted flood maps at (a) $t = 48$ h; (b) $t = 72$ h; (c) $t = 96$ h; (d) $t = 120$ h.

Table 3
The adopted manning coefficients for different types of land use.

Land use type	Manning coefficient ($sm^{-1/3}$)
Mountain	0.15
Sub-urban	0.13
Arable	0.125
Grassland	0.075
Woodland	0.16
Urban	0.03
Fresh water	0.015

pose of this case study is to test the numerical stability and efficiency of the current scheme, the model is not calibrated for the simulations and the used parameters may not represent an optimal parameter set.

The models implemented respectively with the current friction discretisation scheme and IFM are used to simulate this event. Similar to the previous test cases, the two models predict identical simulation results, which is as expected. The predicted flood maps at different output times are presented in Fig. 8. At $t = 48$ h, streams and river channels inside the catchments have already been filled with water. Significant inundation can be observed in the downstream areas. At $t = 72$ h, the flood water has been further routed into the main rivers as indicated by the extended inundation areas and the retreat of water in the upland streams. At $t = 96$ h, the flood peak has passed, and smaller inundated

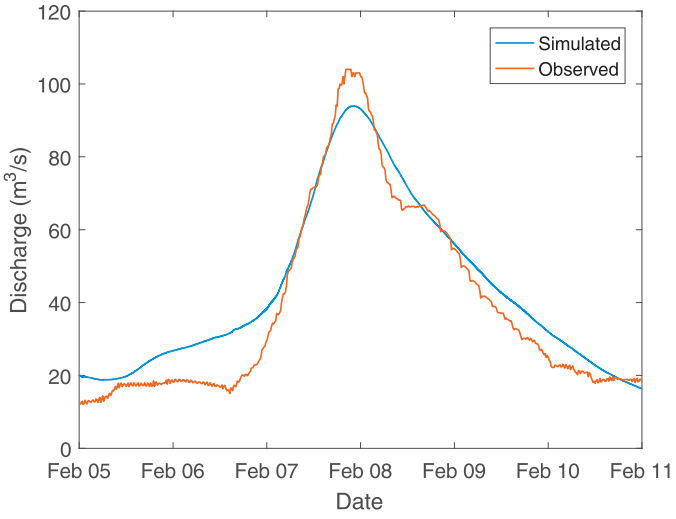

Fig. 9. Comparison between the simulated and observed discharge hydrographs at the catchment outlet.

Table 4
Runtimes consumed by the two friction term discretisation schemes.

Model	Total Runtime	Runtime for friction calculation
Current	153.0 min	4.3 min
IFM	159.5 min	10.1 min
Ratio	1.041	2.35

areas are observed, compared with 24 h ago. The reduced water depth at $t=120$ h suggests further retreat of the flood. Overall, the simulated flood process is consistent with the rainfall pattern, in which most of rain has fallen before $t=96$ h. The predicted discharge hydrograph at the catchment outlet is compared with the observation in Fig. 9. Overall good agreement is achieved between the numerical prediction and the observation except for the slightly over-estimated rising limb at the initial stage. The Nash-Sutcliffe efficiency (NSE) has been adopted herein to quantitatively confirm the accuracy of the numerical prediction. The NSE is defined as

$$NSE = 1 - \frac{\sum_1^N \left(Q_m^n - Q_o^n\right)}{\sum_1^N \left(Q_m^n - \bar{Q}_o\right)}, \tag{45}$$

where N is the total number of time steps, Q_o^n is the observed discharge at $t=n$, Q_m^n is the simulated discharge at $t=n$, and $\bar{Q}_o$ is the mean observed discharge. $NSE=1$ suggests perfect agreement between the prediction and the observation. For this simulation, the NSE is calculated to be 0.91, indicating that the observed discharge has been successfully reproduced with high accuracy by the current model.

To compare the computational efficiency, both of the numerical schemes (i.e. the current scheme and IFM) are implemented in the same GPU-accelerated codebase, which are run in parallel on 4 NVIDIA Tesla K40 GPUs and 2 NVIDIA Tesla K80 GPUs. The runtimes are summarised in Table 4. Considering only the runtime for friction calculation, the current scheme is 2.35 times faster than the IFM. This confirms that the friction discretisation scheme based on the explicit formulae derived in this work is computationally more efficient than IFM embedded with a Newton–Raphson iteration method.

6. Conclusions

This work presents and validates a novel implicit scheme for discretising the stiff friction terms in the 2D SWEs. The scheme features with the following two key properties:

(1) The scheme is able to resolve the relaxation of flow velocities towards the exact steady state determined by the balance between friction and gravity along the flow direction using time steps controlled only by the CFL condition for the overall explicit SWE model;
(2) The scheme can be implemented explicitly without necessity of using any iteration methods.

These properties are crucial to ensure numerically stable, efficient and accurate simulation of very shallow flows, such as overland flows and wet/dry fronts, and the associated processes including soil erosion and solute transport. However, existing friction discretisation schemes usually do not simultaneously possess both of these properties.

The current scheme has been successfully validated against two benchmark tests with satisfactory results, confirming its superior numerical stability and accuracy in comparison with the existing mainstream approaches. The resulting SWE model is then further applied to simulate a rainfall-flooding event in the Upper Lee catchment, UK to further confirm its numerical stability and computational efficiency for the simulation of overland flows and flooding over complex real-world topography. Although the current scheme is proposed in the context of a Godunov-type finite volume method, in principle it can also be used in other numerical methods, e.g. finite difference method and finite element method.

Acknowledgements

This work is funded by the NERC SINATRA and TENDERLY projects (Grant No. NE/K008781/1) and Flood-PREPARED project (Grant No. NE/P017134/1).

References

Audusse, E., Bouchut, F., Bristeau, M.-O., Klein, R., Perthame, B., 2004. A fast and stable well-balanced scheme with hydrostatic reconstruction for shallow water flows. SIAM J. Sci. Comput. 25, 2050–2065. https://doi.org/10.1137/S1064827503431090.
Berger, M.J., George, D.L., LeVeque, R.J., Mandli, K.T., 2011. The GeoClaw software for depth-averaged flows with adaptive refinement. Adv. Water Resour. 34, 1195–1206. https://doi.org/10.1016/j.advwatres.2011.02.016.
Bermudez, A., Vazquez, M.E., 1994. Upwind methods for hyperbolic conservation laws with source terms. Comput. Fluilds. 23, 1049–1071.
Burguete, J., García-Navarro, P., Murillo, J., 2008. Friction term discretization and limitation to preserve stability and conservation in the 1D shallow-water model: application to unsteady irrigation and river flow. Int. J. Numer. Methods Fluids 58, 403–425. https://doi.org/10.1002/fld.1727.
Busaman, A., Mekchay, K., Siripant, S., 2015. Dynamically adaptive tree grid modeling for simulation and visualization of rain-water overland flow. Int. J. Numer. Methods Fluids. https://doi.org/10.1002/fld.4064.
Cea, L., Blade, E., 2015. A simple and efficient unstructured finite volume scheme for solving the shallow water equations in overland flow applications. Water Resour. Res. 51, 5464–5486. https://doi.org/10.1002/2014WR016259.
Cea, L., Garrido, M., Puertas, J., 2010. Experimental validation of two-dimensional depth-averaged models for forecasting rainfall-runoff from precipitation data in urban areas. J. Hydrol. 382, 88–102. https://doi.org/10.1016/j.jhydrol.2009.12.020.
Chow, V.T., 1959. Open Channel Hydraulics.. McGraw-Hill B. Co. doi:ISBN 07-010776-9.
Costabile, P., Costanzo, C., MacChione, F., 2013. A storm event watershed model for surface runoff based on 2D fully dynamic wave equations. Hydrol. Process. 27, 554–569. https://doi.org/10.1002/hyp.9237.
Di Giammarco, P., Todini, E., Lamberti, P., 1996. A conservative finite elements approach to overland flow: the control volume finite element formulation. J. Hydrol. 175, 267–291. https://doi.org/10.1016/S0022-1694(96)80014-X.
Fiedler, F.R., Ramirez, J.A., 2000. A numerical method for simulating discontinuous shallow flow over an infiltrating surface. Int. J. Numer. Methods Fluids 32, 219–240. https://doi.org/10.1002/(SICI)1097-0363(20000130)32:2<219, AID-FLD936>3.0.CO;2-J.
Hou, J., Liang, Q., Simons, F., Hinkelmann, R., 2013. A 2D well-balanced shallow flow model for unstructured grids with novel slope source term treatment. Adv. Water Resour. 52, 107–131. https://doi.org/10.1016/j.advwatres.2012.08.003.
Juez, C., Caviedes-Voullième, D., Murillo, J., García-Navarro, P., 2014. 2D dry granular free-surface transient flow over complex topography with obstacles. Part II: numerical predictions of fluid structures and benchmarking. Comput. Geosci. 73, 142–163. https://doi.org/10.1016/j.cageo.2014.09.010.
Juez, C., Murillo, J., García-Navarro, P., 2013. 2D simulation of granular flow over irregular steep slopes using global and local coordinates. J. Comput. Phys. 255, 166–204. https://doi.org/10.1016/j.jcp.2013.08.002.
Kao, H.-M., Chang, T.-J., 2012. Numerical modeling of dambreak-induced flood and inundation using smoothed particle hydrodynamics. J. Hydrol. 448–449, 232–244. http://dx.doi.org/10.1016/j.jhydrol.2012.05.004.

Liang, D., Falconer, R.A., Lin, B., 2006. Comparison between TVD-MacCormack and ADI-type solvers of the shallow water equations. Adv. Water Resour. 29, 1833–1845. https://doi.org/10.1016/j.advwatres.2006.01.005.

Liang, D., Lin, B., Falconer, R.A., 2007. Simulation of rapidly varying flow using an efficient TVD–MacCormack scheme. Int. J. Numer. Methods Fluids 53, 811–826. https://doi.org/10.1002/fld.1305.

Liang, Q., Marche, F., 2009. Numerical resolution of well-balanced shallow water equations with complex source terms. Adv. Water Resour. 32, 873–884. http://dx.doi.org/10.1016/j.advwatres.2009.02.010.

Murillo, J., García-Navarro, P., 2012a. Augmented versions of the HLL and HLLC Riemann solvers including source terms in one and two dimensions for shallow flow applications. J. Comput. Phys. 231, 6861–6906. https://doi.org/10.1016/j.jcp.2012.06.031.

Murillo, J., García-Navarro, P., 2012b. Wave Riemann description of friction terms in unsteady shallow flows: Application to water and mud/debris floods. J. Comput. Phys. 231, 1963–2001. https://doi.org/10.1016/j.jcp.2011.11.014.

Rousseau, M., Cerdan, O., Delestre, O., Dupros, F., 2015. Overland flow modelling with the shallow water equation using a well balanced numerical scheme: better predictions or just more complexity? J. Hydrol. Eng. 20, 4015012. https://doi.org/10.1061/(ASCE)HE.1943-5584.0001171.

Sanders, B.F., Schubert, J.E., Detwiler, R.L., 2010. ParBreZo: a parallel, unstructured grid, Godunov-type, shallow-water code for high-resolution flood inundation modeling at the regional scale. Adv. Water Resour. 33, 1456–1467. https://doi.org/10.1016/j.advwatres.2010.07.007.

Simons, F., Busse, T., Hou, J., Özgen, I., Hinkelmann, R., 2014. A model for overland flow and associated processes within the hydroinformatics modelling system. J. Hydroinform. 16, 375–391.

Singh, J., Altinakar, M.S., Ding, Y., 2015. Numerical modeling of rainfall-generated overland flow using nonlinear shallow-water equations. J. Hydrol. Eng. 20, 4014089. https://doi.org/10.1061/(ASCE)HE.1943-5584.0001124.

Song, L., Zhou, J., Li, Q., Yang, X., Zhang, Y., 2011. An unstructured finite volumemodel for dam-break floods with wet/dry fronts over complex topography. Int. J. Numer. Methods Fluids 67, 960–980. https://doi.org/10.1002/fld.

Toro, E.F., 2001. Shock-capturing Methods For Free-Surface Shallow flow.. John Wiley & Sons, Ltd.

Xia, X., Liang, Q., 2018. A new depth-averaged model for flow-like landslides over complex terrains with curvatures and steep slopes. Eng. Geol. 234, 174–191. https://doi.org/10.1016/j.enggeo.2018.01.011.

Xia, X., Liang, Q., Ming, X., Hou, J., 2017. An efficient and stable hydrodynamic model with novel source term discretisation schemes for overland flow simulations. Water Resour. Res. 53, 3730–3759. https://doi.org/10.1002/2016WR020055.

Xing, Y., Shu, C.W., Noelle, S., 2011. On the advantage of well-balanced schemes for moving-water equilibria of the shallow water equations. J. Sci. Comput. 48, 339–349. https://doi.org/10.1007/s10915-010-9377-y.

Yu, C., Duan, J., 2017. Simulation of surface runoff using hydrodynamic model. J. Hydrol. Eng. 1–12. https://doi.org/10.1061/(ASCE)HE.1943-5584.0001497.

Yu, C., Duan, J., 2014. Two-dimensional hydrodynamic model for surface-flow routing. J. Hydraul. Eng. 140, 1–13. https://doi.org/10.1061/(ASCE)HY.1943-7900.0000913.

Zhou, J.G., Causon, D.M., Mingham, C.G., Ingram, D.M., 2001. The surface gradient method for the treatment of source terms in the shallow-water equations 168, 1–25. https://doi.org/10.1006/jcph.2000.6670.